Al-Nisour Journal for Medical Sciences

Manuscript 1140

Automated Retinal Vessel Analysis: A Novel Model for Blood Vessel Detection, Segmentation, and Clinical Characteristic Quantification

Aws A. Abdulsahib

Moamin A. Mahmoud

Sally A. Al-Hasnawi

Ahmed Zeyad Almhanna

Jamal Kamil K. Abbas

Scan the QR to view the full-text article on the journal website

Automated Retinal Vessel Analysis: A Novel Model for Blood Vessel Detection, Segmentation, and Clinical Characteristic Quantification

Aws A. Abdulsahib [a], Moamin A. Mahmoud [b], Sally A. Al-Hasnawi [c], Ahmed Zeyad Almhanna [d], Jamal Kamil K. Abbas [e,*]

[a] Computer Science Department, Dijla Universty College, Baghdad, Iraq
[b] College of Computing and Informatics, Universiti Tenaga Nasional, Selangor, Malaysia
[c] Faculty of Information Technology, Al-nahrain University, Baghdad, Iraq
[d] Media Department Decision, Dijla Universty College, Baghdad, Iraq
[e] Cybersecurity Engineering Techniques, Al-Nisour University College, Iraq

Abstract

This research enlightens into a fully automated model for segmenting blood vessels and extracting clinical features from retinal fundus images, which is vital for diagnosing ophthalmologic and cardiovascular diseases. The model utilises contrast enhancement, noise reduction, edge detection, and a method for reconnecting blood vessel branches. It extracts properties like tortuosity, girth, and length of blood vessels. The model's performance surpasses existing approaches, achieving high accuracy, sensitivity, specificity, and positive and negative prediction values on DRIVE and HRF datasets. This innovation offers the potential to reduce specialists' workload, enhance diagnostic accuracy, and streamline the analysis of complex fundus images, ultimately improving patient care.

Keywords: Retinal vessel analysis, Medical image processing, Clinical features characterisation, Automated segmentation, DRIVE, HRF

1. Introduction

Medical research has intensively studied numerous aspects, characteristics, and applications of retinal vessels. Notable research fields include image registration, optical disc detection, change detection, pathology identification and quantification, video sequence tracking, and computer-assisted screening. The comprehensive evaluation of ophthalmologic in addition to cardiovascular disorders depends on quantitative analysis of retinal fundus images. The method of transmission for these image types enables their incorporation into expansive, scalable models. In addition, it allows for enhancing images and the execution of qualitative and quantitative analyses using machine learning techniques. In medical image processing, much research has been devoted to extracting precise geometric models of anatomical structures from medical images. These models form the basis for automated applications designed for early disease detection, modeling of bone reconstruction, and security-related tasks. The architecture of the retina's blood vessels aids in the diagnosis of conditions such as hypertension, diabetes, and cardiovascular disease (Abdulsahib *et al.*, 2021). Imaging the structure of the retinal blood vessels functions as a diagnostic, monitoring, and documentation tool for abnormal conditions (Lal *et al.*, 2021). Recent technological advances have enabled the generation of quantitative signals useful for detecting optic diseases such as glaucoma and diabetic retinopathy, as well as diverse neurovascular and cardiovascular disorders. A comprehensive overview of retinal imaging and its medical implications can be found in Balasubramanian & Ananthamoorthy (2019).

Received 6 January 2025; accepted 8 April 2025.
Available online 9 May 2025

* Corresponding author.
E-mail addresses: aws.abdulkareem@duc.edu.iq (A. A. Abdulsahib), moamin@uniten.edu.my (M. A. Mahmoud), Sally.a.karim@nahrainuniiv.edu.iq (S. A. Al-Hasnawi), ahmed.ziad@duc.edu.iq (A. Z. Almhanna), jamal.k.eng@nuc.edu.iq (J. K. K. Abbas).

https://doi.org/10.70492/2664-0554.1140

Systematic screening programs facilitate early disease detection and the identification of incipient abnormalities in at-risk patient populations. Manual diagnosis is frequently a bottleneck, given the large data required for extensive screening initiatives. To address the growing workload, computer-assisted diagnostic tools acquire and process retinal images, facilitating high-throughput operations in screening programs. As described in Boudegga *et al.* (2021) and Ramos-Soto *et al.* (2021), various approaches for blood vessel separation from retinal images have been proposed to facilitate automated or semi-automated image analysis by simplifying the analysis of vascular structure. In medical research, the unique characteristics of retinal vessels have been indispensable for the early detection of specific disorders (Maity *et al.*, 2020). Moreover, they are crucial in assessing cardiovascular risk, monitoring retinopathy therapies, and facilitating authentication applications based on vessel patterns (Zebari *et al.*, 2020). This distinctiveness makes blood vessel structures suitable for biometric identification. Most medical research instruments are based on quantitative analyses of retinal vessel characteristics (Tomasz Tarasiewicz & Kawulok, 2020). These instruments facilitate the study of the relationship between retinal microvasculature and the diagnosis of diabetes and cardiovascular diseases. Given their potential for significant resource conservation, these diagnostic models can be incorporated into large-scale screening programs. Researchers continue refining algorithms and techniques for accurately and efficiently computing retinal vessel tree features accurately and efficiently from medical images. Despite promising techniques (Dr Rajesh Doss, 2020), the emphasis remains on improving accuracy and computation efficiency, focusing on blood vessel segmentation and characterization in color fundus images.

Utilizing hardware-based approaches for real-time applications can reduce computational time in this context. Identifying the blood vessel structure is the initial step in manual retinal blood vessel segmentation to avoid potential delays in image segmentation caused by manual methods for delineating retinal vessel structures. Consequently, clinical characteristics are utilized for early disease diagnosis and evaluation of treatment (Ramos-Soto *et al.*, 2021). Typically, one of two common cameras is used to acquire the images, as described in Chapter 2. These images are then sent to eye specialists for manual delineation of artery and vein networks without the assistance of computational platforms (Balasubramanian & Ananthamoorthy, 2019). A limitation of this manual approach is the time consumed, particularly when eye specialists analyze numerous images from each patient, each featuring a complex structure that complicates disease stage recognition. Given the dire consequences of delayed eye disease diagnosis, as reported by the World Health Organization (an expected increase in the number of blind individuals from 38.5 million in 2020 to 115 million in 2050) (Soaibuzzaman, 2021), the implementation of automated models in select literature studies aims to speed up the process and enhance disease detection.

The research objectives represented as below:

a) improve diagnostic accuracy and expedite the work of ophthalmologists by developing a hybrid approach that combines precision, speed, and complete automation for retinal fundus image in blood vessel segmentation and evaluation of clinical characteristics. This method emphasises precision, speed, and complete automation
b) precisely identify microscopic blood vessels in retinal images, two fully automated segmentation techniques, trainable and morphological, are presented
c) a novel method for connecting blood vessels is proposed to ensure the proper alignment of segmented blood vessel segments.

2. Related work

Poor quality retinal fundus images analyzed by Gupta and Tiwari (Ali Hatamizadeh & Terzopoulos, 2020) led to enhancing colour retinal images using luminosity and quantile-based contrast enhancement via multidimensional modelling and signal processing. In addition, the proposed model with a peak signal-to-noise ratio of 27.76% and 28.40% yielded the highest average performance. The structural similarity index lost results of 0.66 and 0.69 based on the section's quantity value of three and five pixels, respectively. In 2019, Memari and his team adopted matched filtering and fuzzy c-means clustering with the integrated level set method (CLAHE) to increase image quality and reduce noise (Memari *et al.*, 2018). The accuracy obtained by the authors was 0.961, 0.951, and 0.939%, respectively. The methods limitation of the RVS (retinal vessel segmentation) is the noise due to uneven illumination. The thin artery in the segmented image is also incomplete due to the system's inability to differentiate between the two categories of vessels. The produced image will not contain all types of blood receptacles. If the eye care professional cannot precisely identify the disease, it will substantially affect the diagnosis. In addition, most proposed segmentation methods focused on optimizing the pre-processing and vessel segmentation parameters separately for each dataset. Therefore, the proposed system may not depend on the ophthalmologic decision typically made after physically observing the patient.

Nasser Tamim *et al*. (2020) highlighted hybrid and multi-layer perceptron techniques for vessel networks in 2020, but the works still need improvement. Although the accuracy for DRIVE (Digital Retinal Image Vessel Equalization) is 96.07% and STARE (Structure Analysis Of The Retina) is 96.32%, the results still required 100% accuracy as it involved human welfare. In the medical field, the inaccuracy is considered hazardous. The low sensitivity results recorded in both datasets used for this study resulted in an incorrect diagnosis made by the specialist due to poor image quality. The specialists still need to observe the patient physically to make an accurate diagnosis despite the benefits of the model (Memari *et al*., 2018). Segmentation of retinal blood vessels and deficit detection in blood vessel types was studied for diabetic retinopathy assessment using matched filtering, fuzzy c-means clustering and an integrated level set method. The results demonstrated that techniques could only manage thinner vessels but not thicker vessels. Therefore, an image generated without arteries and veins will be helpful, as the eye care provider can only diagnose the disease with these two essential blood vessels in the retinal fundus image.

Biomedical Signal Processing and Control was also used to construct a fractional filter based on the retinal blood vessel segmentation algorithm due to the difficulties in integrating two image datasets identified by Shukla *et al*. (2020). The average segmentation accuracy of vessels in the STARE and DRIVE databases is 95.73 and 94.76 per cent, respectively. The proposed method is limited by its low sensitivity, which will increase the specialist's burden and further hinder the specialist's ability to diagnose diseases correctly. This may have occurred due to the excision of thin vessels not connected to the main vessels. In addition, false occurred in the pathological image due to the discontinuous branch and segment end connections. Analysis of Reddy (2020) reveals the challenges of extracting clinical characteristics. Their classification accuracy was calculated to be 93.6% in blood vessel extraction from fundus images using hessian eigenvalues and adaptive thresholding to avoid the difficulties of manual segmentation. As they influence the ophthalmologist's decision-making, output evaluations must be close to 100 per cent accurate. This could have an equal impact on the results produced. Therefore, decreased precision will negatively impact patient survival.

3. The proposed model of automated approach for blood vessel segmentation and clinical characteristic measurement

This study presents a novel methodology that integrates fully automated algorithms to detect retinal blood vessels in fundus pictures that pose challenges in analysis. Retinal image analysis is commonly employed in diagnosis, screening, and therapy, particularly in cases involving diabetic retinopathy and macular degeneration, leading to visual impairment. Segmenting blood vessels is necessary for quantitative analysis of retinal pictures. The extraction of clinical features from the segmented vascular tree, such as blood vessel tortuosity, length, density, and thickness, confers notable advantages. Furthermore, the vessels tree holds potential for many medical platforms, such as the analysis of fovea localization. Efforts are underway to create approaches that achieve complete automation in craping and cut-off crucial medical details from RBV (retinal blood vessels). This technology can potentially assist ophthalmologists and eye specialists in identifying and manage diverse retinal illnesses. Fig. 1 illustrates the methodology developed for the segmentation of blood arteries and the measurement of clinical parameters.

3.1. Proposed model

The proposed model aims to enhance diagnosis accuracy and streamline ophthalmologists' workflow by using an automated approach to segment blood vessels and assess clinical parameters in retinal fundus pictures. The model has two main stages: picture segmentation and clinical feature extraction. To accurately identify blood vessels, the segmentation phase utilizes two fully automated methods, namely the morphological and trainable filters. Anisotropic diffusion (A.D.) and Gaussian filtering techniques are employed to optimize the retinal picture for morphological filtering. Subsequently, morphological operations are used to eradicate any undesirable components. An enhanced detector named Canny is used to define all the BV in the retina. The approach of trainable filters responsible on enhance the contrast, visibility, and eliminate noise, of the input image respectively. The image that has been improved is subsequently subjected to segmentation utilizing two innovative segmentation algorithms that rely on the responses of two trainable edge detection filters. The

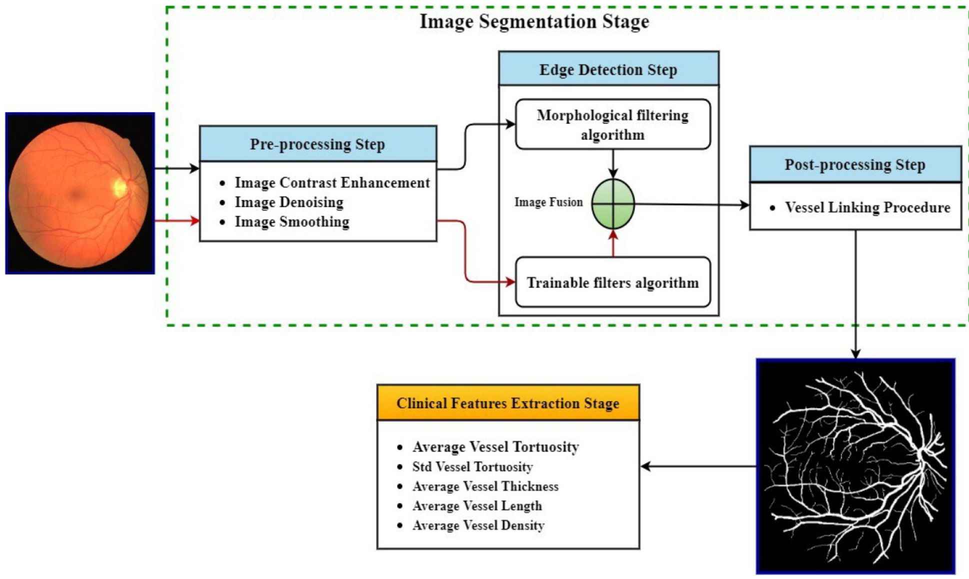

Fig. 1. Proposed methodology for fully-automated blood vessel segmentation and clinical feature measurement.

final segmented image is obtained by merging the segmented images generated by the two presented segmentation techniques. The primary rationale behind integrating these two algorithms lies in their respective capabilities. The first algorithm demonstrates proficiency in detecting the prominent blood vessels in retinal fundus images, while the second method excels in identifying the significantly smaller blood vessels. After the segmentation step, a novel approach establishes connections between blood vessels not connected in the preceding segmented image. The observed clinical manifestation During the extraction step, various clinically relevant features are discovered, including the tortuosity of eye vessel, the arteries and veins length, the density of blood tree, and vessels thickness. These clinical features employed to expedite diagnosing several cardiovascular and ophthalmic disorders. The current acceptable approach for assessing the features of blood arteries involves the determination of their thickness, length, density, and tortuosity.

3.1.1. *The morphological filtering algorithm*

Fig. 2 illustrates the morphological filtering method that has been proposed. The methodology comprises three primary components: picture preprocessing, morphological processes, and vessel identification. The enhanced medical photo was exposed to the morphological process to remove the backdrop and any undesired components, such as short segments of vessels. An enhanced Canny edge detection technique is employed to identify blood vessels within the retinal region. The subsequent sections will provide a detailed explanation of each stage in the proposed morphological filtering algorithm (Abdulsahib *et al*., 2022).

3.1.2. *The trainable filters algorithm*

The proposed trainable filtering system is shown in Fig. 3. It comprises two primary stages: picture preprocessing and vessel identification. During the phase of image pre-processing, a proposed technique is recommended to enhance the quality of the retinal fundus image by mitigating noise and augmenting the blood vessel structure. The process of identifying blood vessels involves the utilization of two trainable filters that possess rotation-invariant properties. These filters, known as the symmetric and asymmetric filters, are employed to capture the responses, which are subsequently combined. The finite medical photo is obtained using a thresholding approach to the hybrid picture (Abdulsahib *et al*., 2022).

3.1.3. *Image fusion step*

The segmented image is produced during the edge detection phase using two innovative segmentation algorithms. These algorithms combine the responses from two trainable filters to accurately and precisely detect the blood vessel structures in the augmented image, as depicted in Fig. 4. Furthermore, the segmented pictures produced by the morphological and trainable filter algorithms are combined using a logical OR function to generate the ultimate segmented image. The primary rationale behind integrating these two algorithms lies in their respective capabilities. The former approach identifies prominent BV

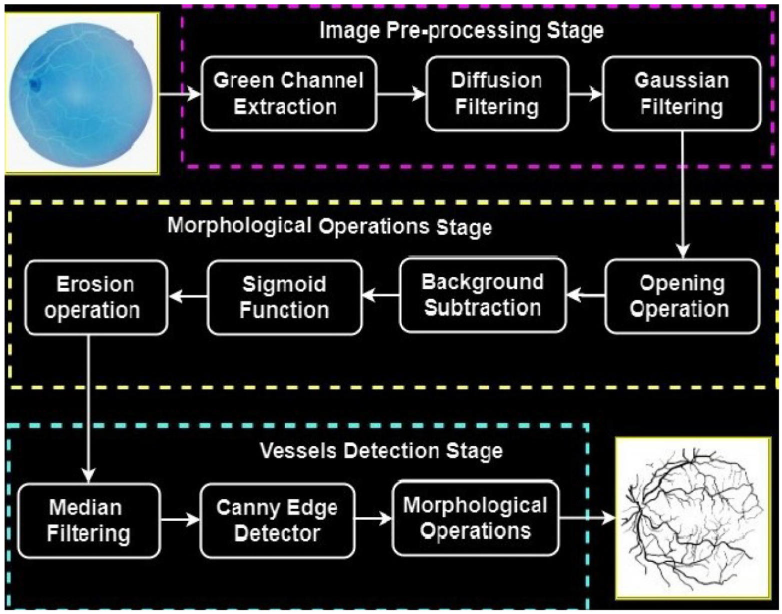

Fig. 2. Stages in recognising retinal blood vessels.

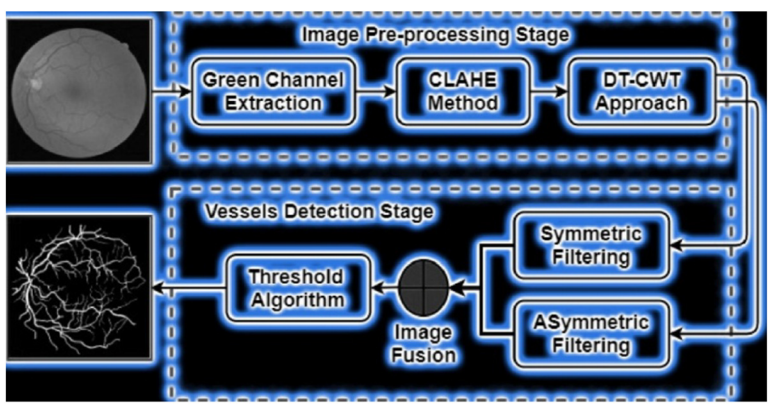

Fig. 3. Proposed trainable filtering method.

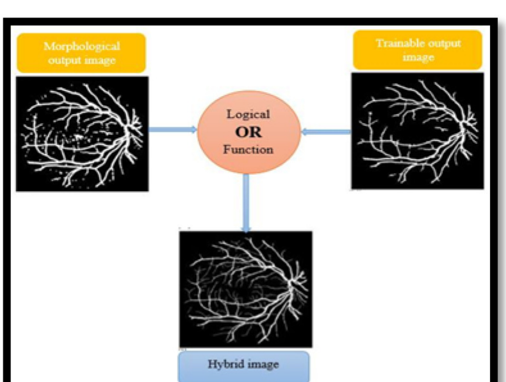

Fig. 4. The image fusion step through utilization of logical OR function.

in medical photos, specifically veins. Meanwhile, the second ones efficiently detects smaller blood vessels, namely arteries. The main objective of employing the hybrid technique and integrating the outcomes of both algorithms is to produce a novel binary retinal fundus image that encompasses a comprehensive vascular tree, including discernible branches of veins and arteries and blood kinds.

Binary images utilize basic logical operators to merge several images. The operator is used on a per-pixel basis. The matching pixel values in the input images determine the pixel values in the resulting image the photos must possess that possess exact dimensions. One primary benefit of utilizing the logical OR operator is its efficiency, as it executes quickly due to its straightforward method. Therefore, the logical

OR operator frequently merges two images, typically binary.

3.2. Post-processing procedure

Obtaining a segmented retina image involves utilizing morphological and trainable filter algorithms. To generate the final segmented image, a hybrid phase is utilized. The final segmented image may have unconnected blood vessels, which can be attributed to their imperceptibility or the presence of noise in the retinal image. This may pose challenges in acquiring precise data on blood vessel dimensions, density, and curvature. To address this issue, a novel approach is suggested to effectively link impaired blood arteries.

The proposed approach for establishing connections between blood vessels involves first constructing the framework of the blood vessels inside the segmented image of the retina same as shown in Fig. 5(a). Followed by identifying the points at which the vessels conclude. Subsequently, the maximum distance between the endpoints of the two severed blood vessel segments is ascertained. A circular structural element with a radius equivalent to half the total length is located at the terminal end of every blood vessel to link impaired blood arteries effectively Fig. 5(b). If two blood arteries converge, their component structures exhibit similar characteristics. Fig. 5(c) illustrates this particular phase. Subsequently, the technique mentioned above is implemented on the complete image, creating a slender line of only one pixel in width. This line serves the purpose of connecting the vessel's two endpoints while also accounting for the attenuated structural components. Consequently, as depicted in Fig. 5(d), the segmented extremities are restored to their initial shape.

3.3. Clinical features extraction stage

Ophthalmologists and other eye specialists can assess the thickness, length, and visual characteristics of retinal lesions resulting from cardiovascular and retinopathy ailments by diagnosing retinopathy diseases. The statistical analysis of vascular tortuosity enables the evaluation of the severity of structural defects in blood vessels and facilitates the identification of optimal treatment strategies. This endeavour aims to develop a comprehensive automated model to accurately segment and extract clinical characteristics from the complete retinal vascular network in fundus images in real time. The clinical feature extraction process precisely and objectively analyses the significant clinical characteristics of the retinal blood vessels that have been automatically detected. At this stage, numerous clinical variables on the health of the retinal blood vessels, such as vascular thickness, length, and appearance, are obtained.

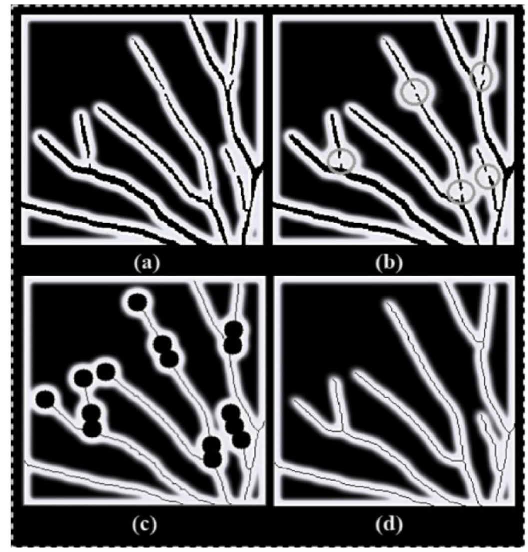

Fig. 5. Method proposed for connecting blood vessels: (a) segmented vascular structures in (b), disjointed blood vessels are represented by red circles, whereas in (c), binary circular components are pasted on every single vessel (d) depicts the final medical photo containing interconnected.

3.3.1. The length of vessel

The length of each segment of the retinal blood vessel is estimated by Eq. (10), which utilises the vessel's skeletal structure as a starting baseline and subsequently incorporates the distances between consecutive pixels inside the segment.

$$Vessel\ Lengh = \sum_{i=1}^{N-1} \sqrt{(x_{i-1} - x_i)^2 + (y_{i-1} - y_i)^2} \qquad (1)$$

The number of pixels inside a row is obtained from the segment's skeletal structure. It also indicates the coordinates of the existing pixels within selected section.

3.3.2. The density of vessel

The measurement of retinal blood vessel density in Eq. (11) includes the division of the aggregate number of pixels included within the blood vessels by the total number of pixels encompassed in the retinal image. This metric offers an assessment of the relative extent to which blood vessels occupy the retinal picture.

$$Vessel\ Density = \frac{\sum The\ vessel\ pixels}{ImageArea\ (mm^2)} \qquad (2)$$

3.3.3. The vessel's curvature

Fig. 6 shows the use of the tortuosity coefficient as a metric for quantifying the extent of curvature

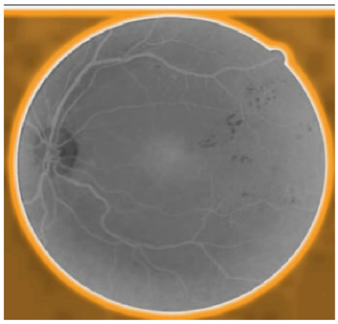

Fig. 6. Blood vessels in the retina of (NPDR) sick condition are extremely convoluted (Joshi, 2012; Abdulsahib et al., 2022).

and torsion present in the trajectory of a blood vessel. A potential association could exist between the tortuosity coefficient of blood vessels and the average internal blood pressure. However, this association demonstrates statistical significance when the critical threshold for blood pressure is attained (Kylstra, 1986, Martynas *et al.*, 2007). The initial step in partitioning a blood vessel segment into branches using a designated equation involved the generation of the blood vessel's skeleton is shown in Eq. (12).

$$BVS = s_1 + s_2 + \cdots + s_b \tag{3}$$

The BVS tortuosity coefficient index was then determined using equation (13):

$$TC\,(BVS) = \sum_{n=1}^{b} s_{length}\,(n) / s_{\text{straight}}\,(n) \tag{4}$$

where s_{length} refers to the length of vessel branch Eq. (12).

$s_{straight}$ is the straightforward distance (14):

$$s_{\text{straight}} = \sqrt{(x_N - x_1)^2 + (y_N - y_1)^2} \tag{5}$$

In this context, N represents the basic vessel pixels, whilst x and y represent the assortment pixel in the section.

3.3.4. The profundity of the vessel

As illustrated in Fig. 7(a), the measurement of retinal blood vessel girth, namely the average breadth of the vessels, was determined by utilizing a novel method developed within the scope of this research. By identifying the precise position of each blood vessel, a series of sequential procedures were performed to establish and refine this method. Initially, a range conversion was applied to the dual representation of the identified BV to ascertain the space between every black pixel in the selected section of medical image and its nearest non-black one. Next, the range conversion utilized on the binary image's converse to compute Euclidean distance or range conversion between every pixel and the closest border pixel in artery. The pixels that exhibited the most significant disparity values were strategically placed near the center of the segment, and distance values indicating the midpoint of the segment were subsequently computed. Determining the blood vessel's half-width involved calculating the mean value of all distance measurements, while the thickness was obtained by multiplying the average value by two as mentioned in Fig. 7(b).

4. Experimental results and discussion

The proposed method was evaluated using two complex datasets, namely the DRIVE D.Y. (2021) and the High-Resolution Fundus (H.R.F.) (Jan Odstrcilik *et al.*, 2013). These datasets were utilized to assess the method's effectiveness in detecting blood vessels in the retina, employing manual and automatic segmentation techniques. Many comprehensive experiments were undertaken to determine the algorithm's performance. The initial step in the project involved the disclosure of the retinal imaging databases. Furthermore, a thorough analysis was conducted to evaluate the efficacy of trainable filters and morphological techniques for automated segmentation. The performance of these methods was compared to that of Ground Truth (G.T.) images. Ultimately, a comparative analysis was conducted to assess the effectiveness of the created algorithms concerning contemporary methodologies. This study aimed to evaluate the accuracy and efficacy of segmentation algorithms when applied to these complicated datasets.

4.1. The characterization of the dataset

The proposed blood vessel segmentation approaches were evaluated using two widely recognized retinal imaging datasets, DRIVE and H.R.F. The datasets are essential because they include images that align with the ground truth (G.T.), comprising blood vessels that medical professionals have manually annotated. This enables the validation of the algorithm's outputs by comparing them to the GT) images, so ensuring their accuracy and use.

The DRIVE (Joshi, 2012) dataset comprises a collection of forty retinal pictures in colour, separated into two distinct groups for training and testing purposes as illustrated in Fig. 8. The DRIVE database comprises retinal images obtained from 400 individuals diagnosed with diabetes in the Netherlands. Among these individuals, 33 do not exhibit any signs of diabetic retinopathy, whereas seven individuals present with moderate early-stage of mentioned disease. Fig. 8 shows a comparative display of internal parts of

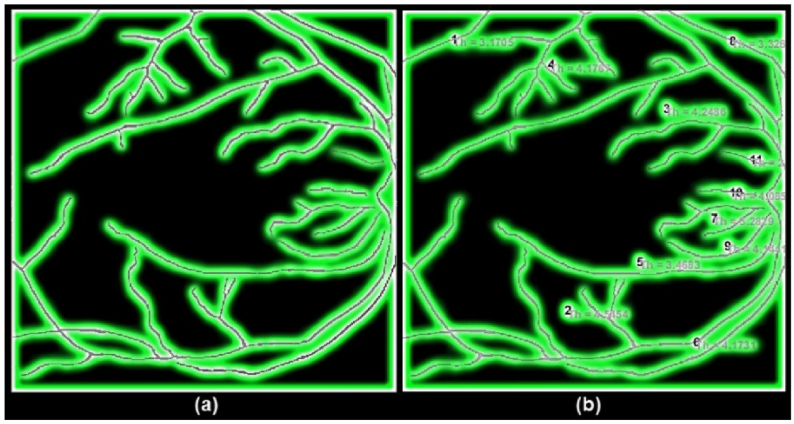

Fig. 7. Results of the established thickness method: (a) Color-coded labeled blood vessels in the retina, and (b) Image representation of retinal blood vessels with their indices and mean thickness measurements.

images generated from first dataset used in this paper, compared with specialist detections acquired standard medical photos.

The dataset referred to as HRF (D.Y., 2021; Li *et al.*, 2016) has 45 images categorised into three distinct groups: healthy individuals, patients diagnosed with diabetic retinopathy, and patients diagnosed with glaucoma. The acquisition of 15 images for each group was conducted using a Canon camera (CF) model with a 60-degree. The pixel size of the images were 6.05 by 6.46 metres, with a resolution of 3504 $\times$ 2336 pixels as illustrated in Fig. 9(a). The dataset comprises binary field-of-view (FOV) mask pictures that are utilised for conducting analysis exclusively inside the borders of the black background Fig. 9(b). In the context of this dataset, a group of three experts diligently delineated the complex structure of blood vessels present in retinal fundus images Fig. 9(c). Fig. 9 illustrates an instance of retinal fundus images sourced from the HRF dataset, accompanied by corresponding gold standard images manually generated.

4.2. *Vessels portion valuation*

The proposed algorithm performs bilateral ranking on every pixel within the medical photo, assigning a label to determine whether it belongs to a vessel or not. A pixel is ranked as a right favorable when it is correctly detected as a artery in both the input image and the ground truth (GT) image. A pixel is classified as a false positive when it is detected as a artery in the resulting cut off image but not in the (GT) image. The evaluation of the effectiveness of the suggested algorithms for retinal vascular segmentation involved the utilization of five quantitative performance measures, namely accuracy (acc.), sensitivity Eq. (15), specificity Eq. (16), positive predictive value Eq. (17), and negative predictive value Eq. (18). These measures were employed to assess the performance of the algorithms. The computation of the mean values for these five criteria facilitated the assessment of the efficiency of the algorithms.

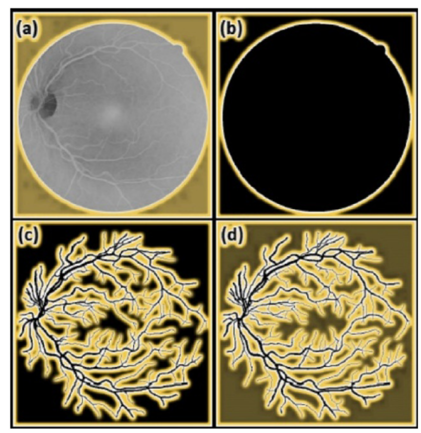

Fig. 8. Eexamples from DRIVE dataset starting by (a) pristine medical photo; (b) combine with mask; (c) produced photo from the first expert; and (d) produced photo from the second expert.

$$\text{Accuracy (Acc.)} = \frac{\text{TP} + \text{TN}}{\text{TP} + \text{FN} + \text{TN} + \text{FP}} \tag{6}$$

$$\text{Sensitivity (Sen.)} = \frac{\text{TP}}{\text{TP} + \text{FN}} \tag{7}$$

$$\text{Specificity (Spe.)} = \frac{\text{TN}}{\text{TN} + \text{FP}} \tag{8}$$

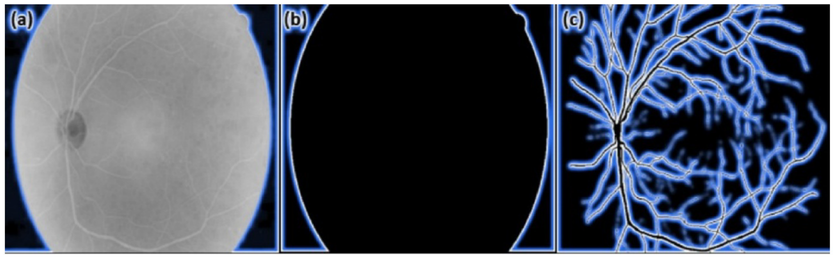

Fig. 9. This medical photo displays (a) initial photo, (b) combine with mask, and (c) specialist detection picture created by an expert from the HRF dataset.

$$\text{Positive Predictive Value (PPV)} = \frac{\mathrm{TP}}{\mathrm{TP} + \mathrm{FP}} \quad (9)$$

$$\text{Negative Predictive Value (NPV)} = \frac{\mathrm{TN}}{\mathrm{TN} + \mathrm{FN}} \quad (10)$$

where TP = True Positives, TN = True Negatives, FP = False Positives and FN = False Negatives,

These metrics evaluate the ratio of accurately recognized pixels. The metric of sensitivity measures the algorithm's capacity to identify vessel particles accurately. The metric of specificity evaluates the algorithm's capacity to classify non-vessel pixels with precision correctly non-vessel pixels with precision. Precision refers to the ratio of accurately detected pixels classed as vessels. The Net Present Value metric is primarily used to assess the accuracy of identifying non-vessel or background pixels.

4.3. The produced results by applying DRIVE dataset

The findings of the proposed model are presented in Table 1. The five evaluations demonstrate that the performance of the second human observer outperformed that of the first. The second observer achieved an accuracy score of 99.55 per cent, a sensitivity score of 99.93 per cent, a specificity score of 93.09 per cent, a positive predictive value score of 98.45 per cent, and a negative predictive value score of 98.89 per cent. The suggested approach demonstrated a high level of effectiveness, as seen by its overall average scores of 99.05%, 99.30%, 98.58%, 93.06%, and 96.73% on the identical measures. The vessels will be rejoined using specified technique for vascular connection. The efficiency of this technique was assessed by calculating the five metrics before and after the blood vessel linking procedure. Fig. 10 illustrates the segmentation findings for (DRIVE) dataset.

The performance of the proposed model is compared to the current vessel segmentation methods using images from the DRIVE dataset, as depicted in

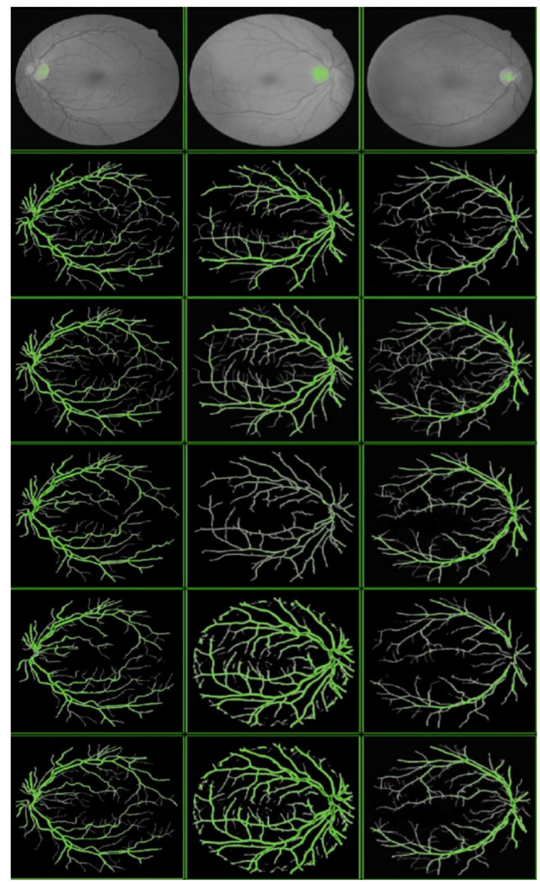

Fig. 10. Performance comparison on the DRVIE dataset.

Table 1. The average quantitative recital metrics of the hybrid approach using the DRIVE dataset.

Evaluation Metrics	First Observer	Second Observer	Rate
Accuracy	98.56	99.55	99.05
Sensitivity	98.67	99.93	99.30
Specificity	98.07	93.09	98.58
PPV	93.67	98.45	93.06
NPV	94.57	98.89	96.73

Fig. 10. The initial row displays the original image. Transitioning to the next row, the visual representation is obtained by the initial human observer. The image acquired by the second human observer is

Table 2. Evaluation metric comparison between proposed model and current vessel segmentation methods.

Methods	Accuracy	Sensitivity	Specificity	P.P.V	N.P.V.
(Jan Odstrcilik *et al.*, 2013)	94.73%	78.07%	97.12%		
(Li *et al.*, 2016)	95.27%	75.69%	98.16%		
(Rothaus *et al.*, 2011)	96.97%	78.94%	98.70%	85.37%	
(Hassan *et al.*, 2015)	96.25%	87.99%	97.99%		
(Houssem & Cherie, 2016)	94.79%	85.06%	95.82%		
(Dasgupta & Singh, 2017)	95.33%	76.91%	98.01%	84.98%	
(Samuel & Veeramalai, 2019)	96.01%	82.20%	97.35%		
(Li *et al.*, 2020)	95.73%	77.35%	98.38%		
(Yang *et al.*, 2018)	95.83%	73.93%	97.92%	77.70%	97.53%
(Kishore & Ananthamoorthy, 2020)	94.10%	69.90%	95.80%	85.50%	94.80%
(Nasser Tamim *et al.*, 2020)	96.07%	75.42%	98.43%	86.34%	96.53%
(Yang *et al.*, 2020)	95.22%	71.81%	97.47%	89.23%	98.50%
(Yang *et al.*, 2019)	94.21%	75.60%	96.96%	78.54%	96.44%
(Keerthiveena *et al.*, 2020)	94.71%	92.7%	95.60%	92.49%	95.70%
The results obtained from this study					
Hybrid Algorithm	99.55%	99.93%	99.09%	93.45%	98.89%

presented in the third row. The output of the morphological filtering method is displayed in the fourth row. The output of the trainable 'filter's algorithm is presented in the fifth row. Ultimately, the output of the hybrid and completely automated process was given in the sixth row.

The data provided by the second human observer was utilized as the benchmark. From the observation, majority of previous research yield outcomes pertaining to accuracy, sensitivity, and specificity. Table 2 presents the regular values of the three measures, together with the positive predictive value (PPV) and negative predictive value (NPV) values. These values were computed by employing a second human observer as the benchmark. Results from current methods had shown greater values for sensitivity and negative predictive value (NPV) in comparison to the proposed model across all five evaluation criteria. However, the proposed hybrid algorithm in this study demonstrated superior performance in general. Majority of the current methods (20, 22, 23, 25, 27, 30, 31, 28) have also reported higher values for sensitivity (SP) and negative predictive value (NPV) compared to the proposed model.

4.4. The produced results of applying HRF dataset

The proposed model was evaluated for vessel segmentation on high resolution fund dataset by means of identical constraint settings as pronounced in Unit 4.2. (G.T.) images sourced from current dataset employed for the suggested model evaluation. The results in Table 3 shown that the proposed hybrid model exhibited superior performance compared to other algorithms by achieving a Net Present Value (NPV) and Positive Predictive Value (PPV) of 100%. Furthermore, the model that was suggested demonstrated superior performance in terms of accuracy (99.95%), sensitivity (99.89%), and specificity (99.78%).

Table 3. Performance comparison on high resolution found dataset.

Evaluation Metrics	Morphological Filtering Algo.	Trainable Filters Algo.	Hybrid Algorithm
Accuracy	98.76	98.78	99.95
Sensitivity	98.87	99.12	99.89
Specificity	99.17	99.34	99.78
PPV	96.88	95.89	100
NPV	100	98.97	100

Fig. 11 depicts a representative example of the outcomes generated by the high-resolution dataset that was discovered. The initial row displayed the original image. Moving to the next row, the visual representation portrayed in the image corresponds to the subjective perception of the human observer. The output segmented image, generated by implementing the proposed morphological filtering technique, is displayed in the third row. Similarly, the fourth row of the presented results displays the output segmented image that has been generated by the algorithm utilising the trainable filters approach. The output segmented image produced by the hybrid and completely automated technique is depicted in the fifth row.

Table 4 compares the proposed model with other common models that are compatible with the HRF dataset. The results of the study revealed that certain segmentation algorithms exhibited superior performance compared to the model that was proposed. An example of this may be seen in the work of Kishore & Ananthamoorthy (2020), where they reached an accuracy of 99.60%. In comparison, the hybrid algorithm described in this study achieved a higher accuracy of 99.95%. However, in contrast to the outcomes of the proposed model, the study outlined in reference

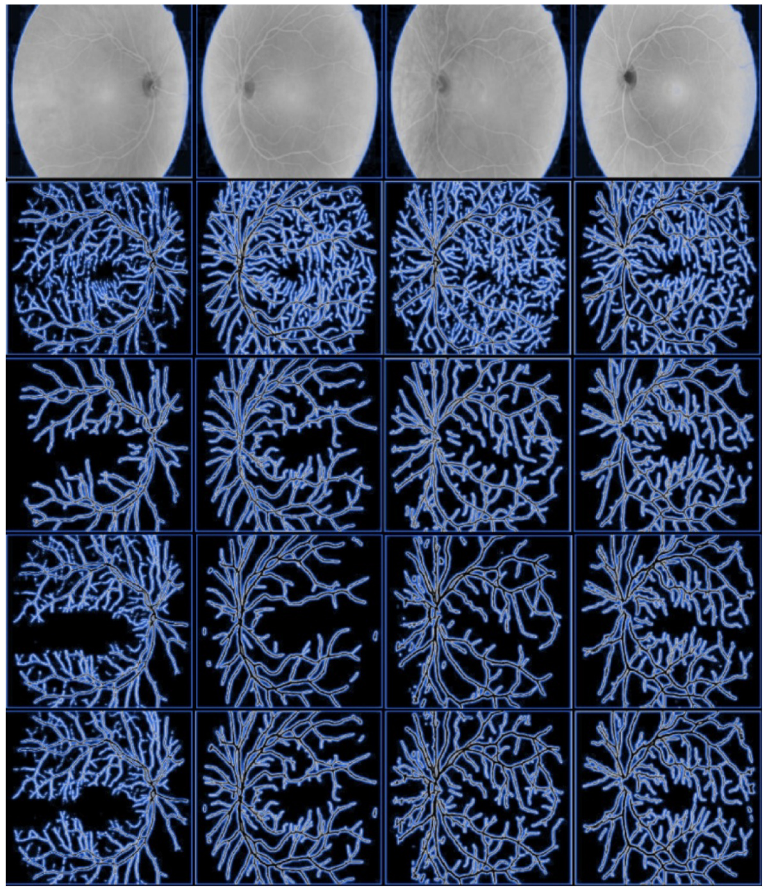

Fig. 11. The segmentation produced results on the high resolution found dataset.

Kishore & Ananthamoorthy (2020) exhibited inferior performance in terms of sensitivity, specificity, positive predictive value, negative predictive value, and other metrics. Additionally, in the study conducted by Chalakkal & Thulaseedharan (2019), a specificity (Spe.) value of 100% was attained, which is marginally greater than the value of 99.78% achieved by the proposed hybrid technique. Nevertheless, their performance on supplementary evaluation measures, such as AC and S.E.N., was subpar. Ultimately, the hybrid algorithm that was proposed demonstrated superior performance compared to contemporary approaches, namely those considered state-of-the-art, when applied to the HRF dataset. The algorithm achieved impressive values for sensitivity (Sen.), accuracy (Acc.), positive predictive value (PPV), and negative predictive value (NPV), with percentages of 99.89%, 99.95%, 100%, and 100% respectively.

In Table 4, a comparison is made between the findings obtained from the proposed model and the existing methods. Furthermore, the numbers presented in this table were obtained from studies which utilized similar measuring methodologies. Consequently, can all be employed to characterize measuring instruments. Based on our analysis and comparison with previous studies, it is evident that the majority of previous studies focused primarily on the segmentation phase. This limited focus suggests that these studies have not fully addressed the comprehensive needs of professionals seeking to make prompt and precise decisions. Given the circumstances, the attention will be directed towards two primary pathways within this investigation: segmentation and extraction of clinical features. Four separate characteristics, namely length, density, tortuosity, and thickness, were the main focus. Nevertheless, the identification of thickness features had not been previously established in the context of this study despite their significant relevance in diagnosing numerous diseases. This is attributed to the limited scope and lack of comprehensiveness in previous research, which often examined singular aspects of the topic. Consequently, the findings derived from these studies proved inadequate

Table 4. Performance comparison between hybrid algorithm and state-of-the-art methods on the HRF dataset.

Methods	Accuracy	Sensitivity	Specificity	P.P.V	N.P.V.
(Vostatek, 2017)	94.30%	58.30%	97.80%		
(Kishore & Ananthamoorthy, 2020)	99.60%	76.52%	98.50%	87.90%	96.00%
(Yang *et al*., 2019)	95.17%	79.15%	96.76%	70.79%	97.90%
(Chalakkal & Thulaseedharan, 2019)	94.40%	88.80%	**100%**		
(Yang *et al*., 2018)	95.49%	72.65%	97.40%	70.03%	97.71%
(Yan & Cheng, 2018)	94.37%	78.81%	95.92%	66.47%	
(Wang *et al*., 2020)	96.54%	78.03%	98.43%		
(Khan *et al*., 2020)	95.90%	77.20%	97.80%		
(Upadhyay & Vashist, 2020)	95.20%	75.00%	97.20%	72.70%	
(Guo & Peng, 2020)	98.56%	80.25%	98.54%		
The results obtained from this research					
Hybrid Algorithm	99.95%	99.89%	99.78%	100%	100%

for eye care providers who sought to utilize them for illness diagnosis. In this undertaking, this study constructs a comprehensive automated model that will encompass the required elements for eye care professionals. This will include segmented fundus images, encompassing the entirety of blood vessel structures and clinical feature data. Physicians will possess the capability to promptly and precisely decide a decision by relying on the outcomes of the proposed model without necessitating a physical examination of the patient.

5. Clinical features evaluation

This section discusses the clinical evaluation procedure employed to assess the accuracy and dependability of the suggested procedures in dig out clinically important characteristics of blood vessels, including tortuosity, length, density, and thickness. These features play a crucial role in the early detection of various cardiovascular and ophthalmologic diseases. The experiment involved comparing the computerized approximations of the four medical characteristics provided by the proposed algorithms with the reference values retrieved from the Ground Truth (G.T.) Images acquired by the first human observer in the datasets utilized. Table 5 presents the statistical measures, including the Mean, Standard Deviation, Maximum, and Minimum values, for each clinical characteristic observed in both the human and automated images. Additionally, the table includes the calculated difference (Diff) and percentage difference (Diff%) between the two sets of images. The proposed hybrid methodology yielded average percentage differences (Diff%) of 7.551%, 0.198%, 0.569%, and 0.736% for the tortuosity, thickness, length, and density, correspondingly, in contrast to the estimations provided by human observers.

The Pearson correlation plots were employed with the first human observer of the DRIVE dataset to demonstrate the effectiveness and reliability of the proposed blood vessel segmentation technique in delivering a precise and automated evaluation of the clinical characteristics of the vessels. The success of the hybrid algorithm was proved by computing Pearson's correlation coefficient (r) and p-values for vessel tortuosity, thickness, length, and density.

The algorithm demonstrated strong correlation coefficients for tortuosity ($r = 0.89$, $p < 0.0001$), thickness ($r = 0.97$, $p \leq 0.0001$), length ($r = 0.86$, $p < 0.0001$), and density ($r = 0.95$, $p < 0.0001$), suggesting nits potential applicability in clinical settings.

Table 5. Comparison of automated and manual approximation of four medical features utilizing the DRIVE dataset's first humanoid spectator.

	Manual	Hybrid Algorithm		
	Tortuosity	Tortuosity	Difference	Difference Percentage
Average	1.814	1.682	0.132	7.551
Standard	0.8628	0.905	−0.042	4.797
Maximum	3.78	4.52	−0.74	17.83
Minimum	1.06	1.02	0.04	3.846
	Thickness	Thickness	Difference	Difference Percentage
Average	3.7735	3.7810	−0.008	0.198
Standard	0.3722	0.3726	−0.0004	0.112
Maximum	4.32	4.22	0.1	2.34
Minimum	2.98	3	−0.02	0.668
	Length	Length	Difference	Difference Percentage
Average	33.447	28.480	0.19	0.569
Standard	4.5592	5.6222	−1.190	23.09
Maximum	47.48	45.28	0.04	0.084
Minimum	28.83	20.13	2.89	10.553
	Density	Density	Difference	Difference Percentage
Average	0.0129	0.0128	−0.0005	0.736
Standard	0.0103	0.0074	0.0028	32.119
Maximum	0.0343	0.0337	0.0006	1.7647
Minimum	0.0025	0.0012	0.0013	70.270

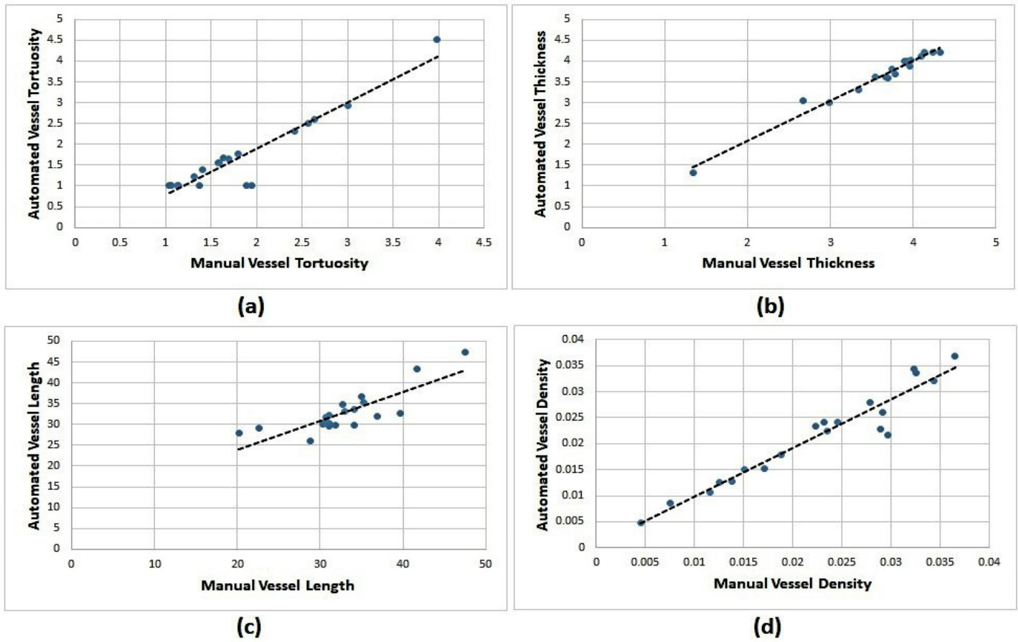

Fig. 12. Correlation analysis of clinical estimates on the DRIVE dataset using proposed hybrid algorithms and manual observations by the first human observer: (a) curvature, (b) thickness, (c) length, and (d) density.

Table 6. Comparison of automatic and manual estimates for four medical traits via the second humanoid spectator from the DRIVE dataset.

	Manual	Hybrid Algorithm		
	Tortuosity	Tortuosity	Difference	Difference Percentage
Average	1.708	1.682	0.026	1.533
Standard	0.903	0.905	−0.0012	0.142
Maximum	4.48	4.52	−0.04	0.888
Minimum	1.01	1.02	−0.01	0.985
	Thickness	Thickness	Difference	Difference Percentage
Average	3.834	3.7810	0.0535	1.405
Standard	0.378	0.3726	0.0061	1.635
Maximum	4.3	4.22	0.08	1.877
Minimum	3.12	3	0.12	3.921
	Length	Length	Difference	Difference Percentage
Average	33.543	28.480	0.2865	0.857
Standard	5.496	5.6222	−0.2536	4.510
Maximum	46.94	45.28	−0.5	1.059
Minimum	26	20.13	0.06	0.231
	Density	Density	Difference	Difference Percentage
Average	0.013	0.0128	0.0004	3.479
Standard	0.007	0.0074	9.6500	1.281
Maximum	0.0344	0.0337	0.0007	2.055
Minimum	0.0013	0.0012	0.0001	8

Table 6 presents findings of the medical assessment performed on the DRIVE dataset, which involved automated assessments of clinical characteristics with a secondary human observer. The hybrid methodology that was proposed showed relative disparities of 1.533%, 1.40%, 0.85%, and 3.47% for the variables of tortuosity, thickness, length, and density, correspondingly. The algorithm being examined was utilized to compare the automated assessments of clinical characteristics with the manual assessments conducted by two human observers. The findings of this study indicated that there were no statistically significant differences identified in the relative values of any clinical characteristic. The maximum relative difference recorded between the two human observers was 4% and 8%, correspondingly. Moreover, it is apparent based on the data presented in Fig. 12 that the algorithm exhibited a higher level of performance when assessed by the second human observer in comparison to the first. This assertion is substantiated by the empirical evidence that the used methodology resulted in noteworthy Pearson's correlation coefficients (r) and p-values for all the clinical characteristics inside the DRIVE dataset.

The proposed hybrid blood vessel segmentation approach was subsequently evaluated on a high-resolution dataset consisting of 40 (G.T) images into measure the performance of the algorithm. Table 7 presents the comprehensive mean, standard deviation, maximum, and minimum values, along with the difference and percentage difference (Diff%) for every clinical trait seen in both human and automated images. The average percentage difference (Diff%) between human and machine estimations for tortuosity,

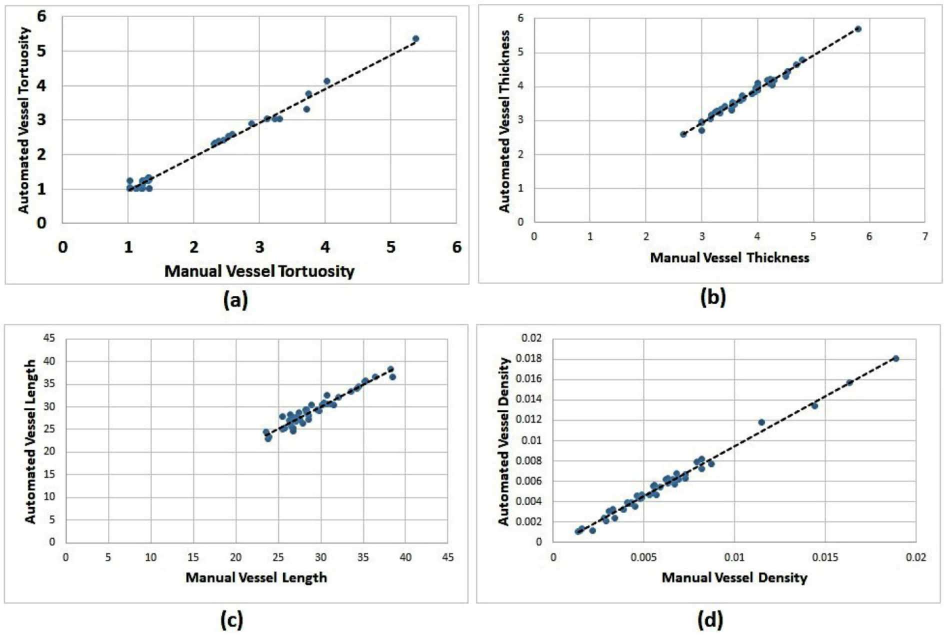

Fig. 13. Four correlation graphs comparing manual and automated clinical evaluations of the high-resolution dataset discovered by the hybrid algorithm (a) tortuosity, (b) thickness, (c) length, and (d) density.

Table 7. A comparison of performance between manual and computerized assessments of the medical characteristics applying the high resolution found dataset.

	Manual	Hybrid Algorithm		
	Tortuosity	Tortuosity	Difference	Difference Percentage
Average	1.580	1.543	0.037	2.376
Standard	0.843	0.859	−0.0168	1.974
Maximum	5.38	5.37	0.01	0.186
Minimum	1.02	1.02	0	0
	Thickness	Thickness	Difference	Difference Percentage
Average	3.834	3.764	0.07	1.842
Standard	0.592	0.5947	−0.0025	0.426
Maximum	5.79	5.69	0.1	1.742
Minimum	2.67	2.61	0.06	2.272
	Length	Length	Difference	Difference Percentage
Average	28.983	28.227	0.756	2.642
Standard	3.673	4.440	−0.7667	18.897
Maximum	38.43	39.96	−1.53	3.909
Minimum	23.56	21.23	2.33	10.404
	Density	Density	Difference	Difference Percentage
Average	0.0059	0.0057	0.0002	3.626
Standard	0.0035	0.0033	0.0002	6.503
Maximum	0.0189	0.0181	0.0008	4.324
Minimum	0.0014	0.0012	0.0002	15.384

thickness, length, and density was found to be 2.376%, 1.842%, 2.642%, and 3.626%, respectively, using the hybrid method described in this study. In general, the disparity between human and computer assessments of clinical traits does not typically exceed 4%. Fig. 13 illustrates the significant correlations observed between the manual and automatic estimations of clinical features utilising the hybrid algorithm proposed in this study. The Pearson's correlation (r) and associated p-values indicate strong correlation, with values of $r = 0.99$ ($p < 0.0001$) for vessel tortuosity, $r = 0.98$ ($p < 0.0001$) for vessel thickness, $r = 0.94$ ($p < 0.0001$) for vessel length, and $r = 0.99$ ($p < 0.0001$) for vessel density.

6. Conclusion

In this paper, a model is developed that can detect blood vessels and quantify clinical characteristics in retinal fundus images automatically. The two primary stages of segmentation are pre-processing and edge identification. The pre-processing phase enhances the contrast of the input image, improves the clarity of the blood vessel architecture, and eliminates noise. The process of edge detection employs two segmentation algorithms to generate a segmented image that effectively discerns the forms of blood vessels. Subsequently, the blood vessels that have undergone image segmentation are interconnected through a method known as blood vessel linkage. During the period of clinical characteristic extraction, this study presents numerous methods for quantifying blood vessel thickness, tortuosity, and length. The effective ness of the proposed model can be determined by evaluating and computing five quantitative performance measures, namely accuracy, sensitivity, specificity, positive predictive value, and negative predictive value. The model demonstrates superior performance compared to current state-of-the-art vessel segmentation algorithms in terms of feature-based accuracy on both the DRIVE and HRF datasets. The proposed model is anticipated to ease the workload of specialists and expedite the process of conceptualization, thereby diminishing the probability of human fallibility.

References

Abdulsahib, A.A., *et al*. (2021) Comprehensive review of retinal blood vessels segmentation and classification techniques intelligent solutions for green computing in medical images, current challenges, open issues, and knowledge gaps in fundus medical images. *Network Modeling Analysis in Health Informatics and Bioinformatics* (2021) 10:20. https://doi.org/10.1007/s13721-021-00294-7. Springer.

Lal, S., *et al*. (2021) Adversarial attack and defence through adversarial training and feature fusion for diabetic retinopathy recognition. *Sensors (Basel)*, 21(11).

Balasubramanian, K., & Ananthamoorthy N.P. (2019) Ananthamoorthy, robust retinal blood vessel segmentation using convolutional neural network & support vector machine. *Journal of Ambient Intelligence and Humanized Computing*, 12(3), 3559–3569.

Boudegga, H., *et al*. (2021) Fast and efficient retinal blood vessel segmentation method based on deep learning network. *Comput Med Imaging Graph*, 90, 101902.

Ramos-Soto, O., *et al*. (2021) An efficient retinal blood vessel segmentation in eye fundus images by using soptimised top-hat and homomorphic filtering. *Comput Methods Programs Biomed*, 201, 105949.

Maity, M., *et al*. (2020) quantification of malaria parasitaemia using trainable semantic segmentation and capsnet. *Pattern Recognition Letters*, 138, 88–94.

Zebari, D.A., *et al*. (2020) Improved threshold based and trainable fully automated segmentation for breast cancer boundary and pectoral muscle in mammogram images. *IEEE Access*, 8, 203097–203116.

Tomasz Tarasiewicz, J.N., & Michal Kawulok (2020) Skinny: A lightweight u-net for skin detection and segmentation. *IEEE*, 978-1-7281-6395-6.

Dr Rajesh Doss. (2020) DeepCNN-A novel deep learning based retinal image segmentation. *Journal of Critical Reviews* ISSN-2394-5125. 7(15).

Soaibuzzaman, PDWH. (2021) Image segmentation based on Convolutional Neural Networks, Chair of Computer Engineering Dept. of Computer Science.

Ali Hatamizadeh, D.S., & Demetri Terzopoulos. (2020) End-to-end trainable deep active contour models for automated image segmentation: Delineating buildings in aerial imagery, computer science department university of california. *Los Angeles*, CA 90095, USA {ahatamiz,debleenas,dt}@cs.ucla.edu.

Memari, N., Ramli, A.R., Saripan, M.I.B., Mashohor, S., & Moghbel M. (2018) "Retinal blood vessel segmentation by using matched filtering and fuzzy c-means clustering with integrated level set method for diabetic retinopathy assessment," *Journal of Medical and Biological Engineering*, 39, 713–731.

Shukla, A.K.R., Pandey, K., & Pachori, R.B. (2020) "A fractional filter based efficient algorithm for retinal blood vessel segmentation," *Biomedical Signal Processing and Control*, 59, 101883.

Prasad Reddy, P.V.G.D. (2020) "Blood vessel extraction in fundus images using hessian eigenvalues and adaptive thresholding," *Evolutionary Intelligence*.

Kylstra l, T.W.J.A., Wolbarsht 1′ 2, M.L., MBB Landers, III 1, & E. (1986) Stefansson a the relationship between retinal vessel tortuosity, diameter, and transmural pressure graefe's arch clin exp ophthalmol, 224, 477–480.

Martynas Patašius, V.M., Arūnas Lukoševičius, Darius Jegelevičius. (2007) Model based investigation of retinal vessel tortuosity as a function of blood pressure: preliminary results. *Proceedings of the 29th Annual International Conference of the IEEE EMBS Cité Internationale, Lyon*, France August 23–26.

Joshi V.S. (2012) Analysis of retinal vessel networks using quantitative descriptors of vascular morphology. *Follow this and Additional Works at: https://ir.uiowa.edu/etd Part of the Biomedical Engineering and Bioengineering Commons*.

Joshi V.S. (2012) Analysis of retinal vessel networks using quantitative descriptors of vascular morphology.pdf. the Biomedical Engineering and Bioengineering Commons.

D.Y. *et al*., (2021) Retinal blood vessel segmentation method based on multi scale convolution kernel U net model. MDPI, *vol. J Northeast Univ (Nat Sci)* 42(1).

Jan Odstrcilik, Radim Kolar, Attila Budai, *et al*. (2013) Retinal vessel segmentation by improved matched filtering: Evaluation on a new high-resolution fundus image data.pdf. *IET Image Process*, 1–11. 1 doi: 10.1049/iet-ipr.2013.0455.

Li Q, Bff, L. Xie, P. Liang, H. Zhang, & Wang T. (2016) A cross-modality learning approach for vessel segmentation in retinal images. *IEEE Trans. Med. Imaging* 35(1), 109–118. doi: 10.1109/TMI.2015.2457891.

Rothaus, K., Jiang, X., Pham, T.D., Zhou, X., Tanaka, H., Oyama-Higa, M., *et al*. (2011) Classification of arteries and veins in retinal images using vessel profile features, 9–18.

Hassan, G., N.E.-B., Hassanien, A.E., Fahmy, A., Abullahm, S., & Snasel V. (2015) Retinal blood vessel segmentation approach based on mathematical morphology. *Procedia Comput. Sci.*, 65, no. Iccmit, 612–622. doi: 10.1016/j.procs.2015.09.005.

Houssem A.C.T.H., & Cherie, B.T.F. (2016) A multi-scale tensor voting approach for small retinal vessel segmentation in high resolution fundus images.pdf. *Comput Med Imaging Graph*, 52: 28–43.

Dasgupta A. & Singh, S. (2017) A fully convolutional neural network based structured prediction approach towards the retinal vessel segmentation. *Proc. - Int. Symp. Biomed. Imaging*, 248–251. doi: 10.1109/ISBI.2017.7950512.

Samuel, P.M., & Veeramalai T. (2019) Multilevel and multiscale deep neural network for retinal blood vessel segmentation. *Symmetry (Basel).*, 11(7). doi: 10.3390/sym11070946.

Li, L., Nakashima, MVV, Y., Nagahara, H., & Kawasaki, R. (2020) IterNet: Retinal image segmentation sutilising structural redundancy in vessel networks. *Proc. - 2020 IEEE Winter Conf. Appl. Comput. Vision, WACV*, 3645–3654. doi: 10.1109/WACV45572.2020.9093621.

Yang, Y., F.S., Fu, Z., & Fu, R. (2018) Blood vessel segmentation of fundus images via cross-modality dictionary learning. *Appl. Opt.*, 57(25), 7287. doi: 10.1364/ao.57.007287.

Kishore, B. & Ananthamoorthy, N.P. (2020) Glaucoma classification based on intra-class and extra-class discriminative correlation and consensus ensemble classifier. *Genomics*, 112(5), 3089–3096. doi: 10.1016/j.ygeno.2020.05.017.

Nasser Tamim., M.E., Gamil Abdel Azim, & Hamed Nassar. (2020) Retinal blood vessel segmentation using hybrid features and multi-layer perceptron neural networks.pdf. *MDPI*, Symmetry, 12, 894; doi:10.3390/sym12060894.

Yang, J., M.H., Fu, J., Lou, C., & Feng, C. (2020) Frangi based multi-scale level sets for retinal vascular segmentation. *Comput. Methods Programs Biomed.*, 197, 105752. doi: 10.1016/j.cmpb.2020.105752.

Yang, Y., Fu, F.S.Z., & Fu, R. (2019) Discriminative dictionary learning for retinal vessel segmentation using fusion of multiple features. *Signal, Image Video Process.* 13(8) 1529–1537. doi: 10.1007/s11760-019-01501-9.

Keerthiveena, B., Selvakumar, S.E.K., & Yogesh, T. (2020) Computer-aided diagnosis of retinal diseases using multidomain feature fusion. *Int. J. Imaging Syst. Technol.* 30(2), 367–379. doi: 10.1002/ima.22379.

Vostatek, P. (2017) Blood vessel segmentation in the analysis of retinal and diaphragm images blood vessel segmentation in the analysis of retinal and diaphragm.

Kishore B. & Ananthamoorthy, N.P. (2020) Glaucoma classification based on intra-class and extra-class discriminative correlation and consensus ensemble classifier. *Genomics*, 112(5), 3089–3096. doi: 10.1016/j.ygeno.2020.05.017.

Yang, F.S.Y., Fu, Z., & Fu, R. (2019) Discriminative dictionary learning for retinal vessel segmentation using fusion of multiple features. *Signal, Image Video Process*. 13(8), 1529–1537. doi: 10.1007/s11760-019-01501-9.

Chalakkal, W.H.A.R.J., & Thulaseedharan, S.S. (2019) Quality and content analysis of fundus images using deep learning. *Comput. Biol. Med.*, 108, no. March, 317–331. doi: 10.1016/j.compbiomed.2019.03.019.

Yang, F.S.Y., Fu, Z., & Fu, R. (2018) Blood vessel segmentation of fundus images via cross-modality dictionary learning. *Appl. Opt.*, 57(25), 7287. doi: 10.1364/ao.57.007287.

Yan, X.Y.Z., & Cheng, K.T. (2018) Joint segment-level and pixel-wise losses for deep learning based retinal vessel segmentation. *IEEE Trans. Biomed. Eng.*, 65(9), 1912–1923. doi: 10.1109/TBME.2018.2828137.

Wang, A.H.D., Pottenburgh, J., Saeedi O., & Tao, Y. (2020) Hard attention net for automatic retinal vessel segmentation. *IEEE J. Biomed. Heal. Informatics*, 24(12) 3384–3396. doi: 10.1109/JBHI.2020.3002985.

Khan, M.S.S.K.B., Ahmad, M., & Mazzara, M. (2020) A hybrid unsupervised approach for retinal vessel segmentation. *Biomed Res. Int.*. doi: 10.1155/2020/8365783.

Upadhyay, M.A.K., & Vashist, P. (2020) Unsupervised multiscale retinal blood vessel segmentation using fundus images. *IET Image Process.*, 14(11), 2616–2625. doi: 10.1049/iet-ipr.2019.0969.

Guo, Y., & Peng, Y. (2020) BSCN: Bidirectional symmetric cascade network for retinal vessel segmentation. *BMC Med. Imaging*, 20(1), 1–22. doi: 10.1186/s12880-020-0412-7.

Aws A. Abdulsahib, Moamin A Mahmoud, Hazleen Aris, Saraswathy Shamini Gunasekaran, Mazin Abed Mohammed. (2022) An automated image segmentation and useful feature extraction algorithm for retinal blood vessels in fundus images. mdpi.com/Electronics 11, 1295. https://doi.org/ 10.3390/electronics11091295.

Aws A. Abdulsahib, Moamin A Mahmoud, Sally A. Al-Hasnawi (2022) An algorithm for shrinking blood receptacles using retinal internal pictures for clinical characteristics measurement. *International Journal of Advanced Computer Science and Applications(IJACSA)*, 13(10).